PAPER

Check for updates

In situ molten phase-assisted self-healing for maintaining fiber morphology during conversion from melamine diborate to boron nitride†

Chunzhi Wu, [ID][a] Bing Wang, [ID]*[a] Nan Wu, [ID][b] Cheng Han,[a] Xiaoshan Zhang[a] and Yingde Wang [ID]*[a]

$C_3N_6H_6 \cdot 2H_3BO_3$ (M·2B) is a highly promising precursor of boron nitride (BN) fibers due to its eco-friendly and low-cost fabrication. However, it is still unclear why the fibers can maintain their morphology in spite of drastic weight loss (nearly 80 wt%) during M·2B-to-BN pyrolysis. Herein, an interesting cracking and self-healing behavior of the heated M·2B fibers was observed at initial pyrolysis. *In situ* formed molten boron oxide (B_2O_3) was figured out to be the healing agent for the cracks and subsequently merged into the continuous matrix enclosing melamine/melem molecules, which subsequently acted as a nitrogen source. The B_2O_3 matrix helped to keep the fiber morphology undamaged under the second weight-loss stage in the pyrolysis process. This strategy of taking advantage of the *in situ* formed molten phase for healing cracks offers detailed guidance to prepare defect-free M·2B-derived BN fibers and would be significant in defect repair for other ceramics.

Introduction

Due to the excellent comprehensive performances of thermal stability, chemical corrosion tolerance, oxidation resistance, neutron absorption, high thermal conductivity, electrical insulation and low dielectric constant,[1–4] hexagonal boron nitride (BN) holds great promise in various fields such as aerospace, high-temperature filtration, nuclear industry, and microelectronics. As typical BN materials, BN fibers similar to anisotropic BNNSs enjoy wide attention owing to their unique properties provided by their high-aspect-ratio morphology.[5,6]

Up to now, numerous fabrication techniques have been developed for the high-efficiency production of BN fibers, which are mostly based on the spinning process that requires strict manipulations.[7–11] In addition, the pyrolysis of a $C_3N_6H_6 \cdot 2H_3BO_3$ (M·2B) supra-molecule adduct is an alternative way and promising for large-scale production owing to the facile and eco-friendly fabrication of M·2B.[12–14]

Unfortunately, the ceramic yield of M·2B is much lower (~20 wt%) than that of other reported polymeric precursors of BN,[15–18] for example, 57 wt% yield of poly[2,4,6-tris(iso-

propylamino)borazine].[17] This implies that substantial release occurs during thermal conversion from M·2B to the final BN fibers. Moreover, M·2B is a supra-molecule constructed by low-strength hydrogen bonding[19,20] that might fail to self-support at a high temperature, resulting in structural collapse. These two disadvantages may cause serious defects in the final BN fibers. The fact, astonishingly, is that the M·2B-derived BN fibers display intact morphology basically inherited from initial M·2B.[13,21] It still remains unclear why the seemingly contradictory phenomenon occurs.

In this work, we observed unique self-healing behavior after morphological cracks were caused by huge weight loss. This self-healing behavior kept the fiber morphology intact, while its micro-structure was drastically broken and reconstructed during pyrolysis. The molten boron oxide (B_2O_3) generated *in situ* from the H_3BO_3 portion was proven to work for healing the cracks and repairing the fiber. Moreover, the boron oxide network could enclose melamine molecules and its condensate melem to prevent them from evaporation, which was crucial to keep the fibers intact as pyrolysis and nitridation proceeded in the subsequent process.

Experimental section

Synthesis of $C_3N_6H_6 \cdot 2H_3BO_3$

A mixture of $C_3N_6H_6$ and H_3BO_3 (analytical reagents, Sinopharm Chemical Reagent Co., Ltd.) with a molar ratio of 1 : 2 was added into de-ionized water and dissolved at 85 °C in a water bath with vigorous stirring; the concentration of $C_3N_6H_6 \cdot (H_3BO_3)$ was set as 0.08 mol L^{-1} (0.16 mol L^{-1}) to ensure

[a]*Science and Technology on Advanced Ceramic Fibers and Composites Laboratory, College of Aerospace Science and Engineering, National University of Defense Technology, Changsha, 410073, P. R. China. E-mail: bingwang@nudt.edu.cn; wangyingde@nudt.edu.cn*

[b]*Department of Materials Science and Engineering, College of Aerospace Science and Engineering, National University of Defense Technology, Changsha, 410073, P. R. China*

complete dissolution. Then, the hot aqueous solution was naturally cooled down to precipitate the $C_3N_6H_6 \cdot 2H_3BO_3$ (M·2B) flocculent. Subsequently, the white flocculent was frozen and dried using a vacuum freeze-dryer (LGJ-FD, Beijing Songyuan Huaxing Technology Develop Co., Ltd, China) to get well-dispersed M·2B fibers.

Thermal treatment of $C_3N_6H_6 \cdot 2H_3BO_3$

The thermal behavior of M·2B was analyzed using thermogravimetry and differential scanning calorimetry (TG-DSC, NETZSCH STA449F5, Germany); the heating rate was set as 10 °C min^{-1}. Based on the results, the M·2B fibers were separately heated to 125 °C, 150 °C, 200 °C, 400 °C, 550 °C, 650 °C, and 1000 °C at the same temperature ramping rate and immediately cooled down. The thermal treatments were conducted in a quartz tubular furnace under a protective N_2 flow. The obtained samples were designated as M·2B$_{125}$, M·2B$_{150}$, M·2B$_{200}$, M·2B$_{400}$, M·2B$_{550}$, M·2B$_{650}$, and M·2B$_{1000}$. For comparison, melamine and boric acid underwent the same TG-DSC testing and were also heated at 150 °C, 200 °C, and 400 °C. To explore the effect of the self-healing process on the morphology of the final BN fibers, the M·2B fibers were also heated under a stage-variable N_2 or NH_3 atmosphere. For example, the M·2B fiber was heated to 700 °C for 1 hour under NH_3 and subsequently heated to 1000 °C under switched N_2.

Characterization and corrosion testing

The morphologies of the samples were observed by field-emission scanning electron microscopy (SEM, Hitachi S-4800, Japan), and the constituents were characterized through Fourier transform infrared spectroscopy (FT-IR, Frontier, PerkinElmer, USA), X-ray diffraction (XRD, Bruker AXS D8 Advance diffractometer, Germany), and ^{13}C nuclear magnetic resonance (NMR) spectroscopy in a DMSO-d$_6$ solvent (400 MHz Agilent 400/54/ASP, USA). The molten transition point of monophasic H_3BO_3 was measured using the melting point apparatus (WRS-2A, Shanghai INESA Physico-Optical Instrument Co., Ltd.).

The corrosion testing of the M·2B$_T$ fiber (T = 150, 200, 400, and 550 °C) was conducted using ethanol (EA) and ethylene glycol (EG) as corrosive agents. Initially, two samples were separately immersed in EA and EG for 1 minute and then taken out for washing 3 times by de-ionized water via a vacuum filtration apparatus. After that, the treated samples were dried over-night in an oven at 80 °C for observing morphology. Furthermore, the M·2B$_T$ fibers (0.02 g) were dipped in 4 ml solvent (EA and EG) for 6 hours to estimate their solubility, which reflected the corrosion resistance of the fibers.

Results and discussion

Morphology transformation

Fig. 1a indicates the thermal behavior of M·2B using TG-DSC; the whole pyrolysis procedure can be divided into two obvious weight-loss stages. In the first stage, in the range of 125–200 °C, there is a sharp endothermic peak at 159.9 °C due to intense weight loss. During the second stage, the gravimetric curve

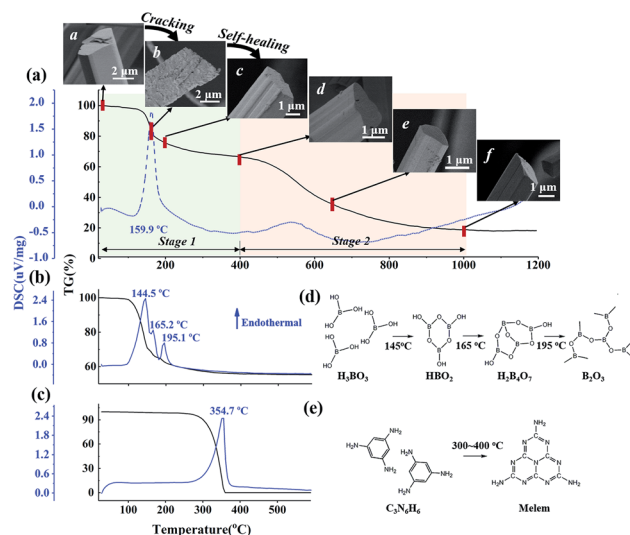**Fig. 1** TG-DSC curves of (a) M·2B supramolecular fibers, (b) H_3BO_3 and (c) $C_3N_6H_6$. In (a), the first weight-loss stage is in the range of 20–400 °C; the second weight-loss stage is in the range of 400–1000 °C, the inset SEM images demonstrate the morphological evolution of the $C_3N_6H_6 \cdot 2H_3BO_3$ fibers during thermal treatment: a M·2B, b M·2B$_{150}$, c M·2B$_{200}$, d M·2B$_{400}$, e M·2B$_{650}$, f M·2B$_{1000}$. (d) Molecular transformation of H_3BO_3 and (e) $C_3N_6H_6$ in the heating process. In (d), H_3BO_3 is converted to metaboric acid (HBO_2) and further to tetraboric acid $H_2B_4O_7$ and finally to a boron oxide structure. In (e), $C_3N_6H_6$ condenses to melem at 300–400 °C.[22]

slowly decreases from 500 to 1000 °C, and a broad weak endothermic peak is located at 535 °C. The insets show the morphology of the M·2B fiber and its thermal products after being heated separately at 150 °C, 200 °C, 400 °C, 650 °C, and 1000 °C; they are designated as M·2B$_{150}$, M·2B$_{200}$, M·2B$_{400}$, M·2B$_{650}$, and M·2B$_{1000}$, respectively. It was obvious that a drastic variation in the fiber's morphology occurred at the first stage; the fiber cracked when heated at 150 °C and self-healed at 200 °C. After this, the fiber got smoother at 400 °C (inset (d) of Fig. 1a) and was intact in the whole second stage (from inset (d) to inset (f) of Fig. 1a). In the final stage, the M·2B$_{1000}$ fiber displayed compact morphology. Thus, self-healing was proven to be the key to maintain the fiber's morphology in spite of the ultralow yield (~20 wt%) of M·2B.

The fiber's cracking could undoubtedly be mainly attributed to the intense weight loss, revealing substantial decomposition at 150 °C, but it was not clear why the self-healing behavior of M·2B$_{200}$ occurred. To explore the reason, the structural transformation during cracking-healing was analyzed.

Considering that M·2B is an adduct of H_3BO_3 and $C_3N_6H_6$ connected via hydrogen bonding,[20] we studied the thermal behavior of the two components separately. Fig. 1b and c display the TG-DSC curves of H_3BO_3 and $C_3N_6H_6$, respectively. It can be found that the same-region weight loss of boric acid occurs (Fig. 1b) as the first-stage weight loss of M·2B. Meanwhile, $C_3N_6H_6$ remained stable at 150–200 °C, as implied by the flat TG curve (Fig. 1c) and the XRD patterns of the heated products (Fig. S1b†).

The weight loss of boric acid could be divided into three stages according to three sharp endothermic peaks, separately corresponding to the different stages of the dehydration of H_3BO_3, as shown in Fig. 1d. These reaction equations were proved by the XRD patterns of the heating products (Fig. S1a†). Thus, the first-stage weight loss of M·2B and the corresponding morphology evolution were basically attributed to the dehydration of H_3BO_3 in M·2B. At the subsequent stage from 200 to 400 °C, there was no obvious weight loss against the sublimation and condensation of melamine (Fig. 1c and e), which would be discussed later. This stable stage ensured that the morphology of the M·2B$_{400}$ fiber became more dense and smooth rather than broken.

Based on the analysis of the thermal transformation of the pure phases of $C_3N_6H_6$ and H_3BO_3, the structural evolution of M·2B involving morphological cracking–healing was further studied using FT-IR spectroscopy and XRD. As shown in Fig. 2a, plenty of sharp peaks disappear after the conversion from M·2B to M·2B$_{150}$, especially in the fingerprint region (marked by the light green rectangle areas) of the hydrogen-bonded structure. The FTIR peaks at 1186 cm^{-1} and 786 cm^{-1} that respectively represents bending and twisting vibrations of B–OH, became feeble as to M·2B$_{150}$. This indicated the drastic removal of hydroxyl groups, which was in accordance with the dehydration of H_3BO_3. Meanwhile, the highly crystallized M·2B was converted into an unordered phase of M·2B$_{150}$ characterized as double broad peaks (Fig. 2b).

M·2B$_{125}$ displays an intermediate structure, revealing the transformation process from M·2B to unordered M·2B$_{150}$, which was characterized as weaker peaks located mainly in the green fingerprint region in the IR spectrum and the co-existence of sharp and broad peaks in the XRD pattern. Therefore, the drastic removal of hydroxyl groups due to the dehydration of H_3BO_3 resulted in the breakage of the M·2B crystal and thus

structural disordering. Morphology cracking could be attributed to the drastic structure transformation and also the huge release of the removed H_2O. As for the micro-structure of the cracked fiber, it should be noted that the sharp XRD peaks of M·2B$_{125}$ correspond well with the (−110), (012), (111) and (102) crystal planes of melamine (ICSD PDF#39-1950) but not M·2B (Fig. 3a). This means that there occurred the assembly of melamine molecules to form crystals, while disordering occurred in the initial M·2B crystal, allowing for the fact that $C_3N_6H_6$ was molecularly isolated by H_3BO_3 in M·2B. Thus, the double broad peaks of M·2B$_{150}$ were proved to result from the widening of the (−110) and (102) diffraction peaks and indicated the existence of melamine micro-crystals in the M·2B$_{150}$ fiber.

From the cracked M·2B$_{150}$ to the healed M·2B$_{200}$, there also occurred intense structural transformation. In addition to the IR peaks belonging to –NH$_2$, C–N, BO$_3$, triazine ring, and B$_3$O$_3$, the evolved peak of BO$_4$ at 1050 cm^{-1} indicates the formation of a B_2O_3 network.[23,26] Two undefined peaks at 1240 cm^{-1} and 1302 cm^{-1} existing for M·2B$_{200-400}$ may be related to the C–O–B structure formed between melamine and boron oxide,[27] which can keep melamine non-volatile in the range of 300–400 °C (Fig. 1a and c). The ^{13}C NMR spectra of monophasic melamine, M·2B, M·2B$_{150}$ and M·2B$_{200}$ (Fig. S2†) also proved the consistent structural evolution, which especially revealed a slight difference between M·2B$_{150}$ and M·2B$_{200}$. The change may be caused by the newly formed carbonaceous structure.

Besides, the double broad XRD peaks of M·2B$_{150}$ merged into an envelope peak of M·2B$_{200-400}$. Interestingly, a broad peak belonging to g-B_2O_3 was located at 23° (Fig. S1a†) between the double broad peaks located at 16.3° and 26.2°. To study this in detail, we fitted the XRD peaks of M·2B$_{150}$, M·2B$_{200}$, and M·2B$_{400}$ using that of g-B_2O_3 as a reference. As shown in Fig. 3b, the envelope peak for the healed M·2B$_{200}$ fiber can be well fitted as the double peaks of M·2B$_{150}$ and a broad peak of g-B_2O_3, and the envelope peak of smoothed M·2B$_{400}$ becomes more
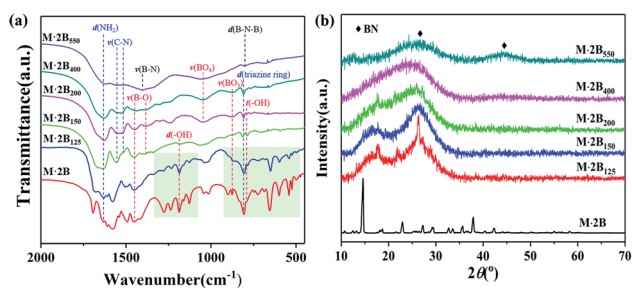
Fig. 2 (a) FT-IR spectra and (b) XRD patterns of the M·2B supramolecule and its heated products M·2B$_{125}$, M·2B$_{150}$, M·2B$_{200}$, M·2B$_{400}$, M·2B$_{550}$. The light green rectangle areas in (a) are the fingerprint region of the hydrogen-bonded adduct structure, and the absorption bands are labeled as follows: d(NH$_2$): –NH$_2$ bending, 1620 cm^{-1}; v(C–N): C–N stretching, 1552 cm^{-1} and 1525 cm^{-1}; v(B–O): 1450 cm^{-1} to B–O asymmetric stretching in BO$_3$ and 1380 cm^{-1} to B–O stretching in B$_3$O$_3$ ring; v(B–N): B–N stretching at 1400 cm^{-1}; d(–OH): –OH bending, 1186 cm^{-1}; v(BO$_4$): B–O stretching in the BO$_4$ unit, 1050 cm^{-1}; v(BO$_3$): B–O symmetric stretching in the BO$_3$ unit, 873 cm^{-1}; d(triazine ring): triazine ring bending at 808 cm^{-1}; d(B–N–B): out-of-plane bending of B–N–B at 802 cm^{-1}; t(–OH): out-of-plane –O–H twisting at 786 cm^{-1}.[23–25]

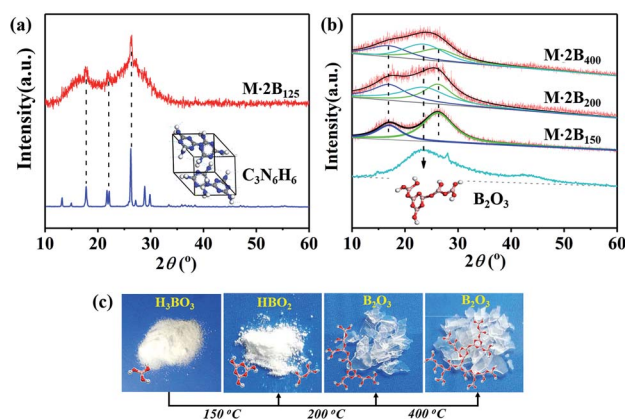**Fig. 3** (a) Analysis of the XRD pattern of M·2B$_{125}$ in comparison with that of melamine. (b) Peak fitting of the XRD patterns of M·2B$_{150}$, M·2B$_{200}$, and M·2B$_{400}$ using B_2O_3 as a reference. (c) Photographs of the original H_3BO_3 and heat treatment products: HBO$_2$ after 150 °C heating, B_2O_3 after 200–400 °C heating, the insets are the corresponding molecular structures.

integrated owing to the more intense peak of g-B_2O_3, while the double peaks belonging to melamine decrease. Therefore, it was confirmed that a g-B_2O_3 phase evolved in $M\cdot 2B_{200-400}$, which may be related to the self-healing of the fiber. Fig. 3c displays the photos of H_3BO_3 and its heated products. Metaboric acid formed at 150 °C was a white powder just like boric acid, but g-B_2O_3 obtained at 200–400 °C turned into a glass-like solid, which revealed that it was melted. The result of the melting point measurement of H_3BO_3 also proved that a viscous phase evolved at 206.2–207.8 °C. Allowing for the same boron–oxygen network in $M\cdot 2B_{200-400}$ as in pure B_2O_3, we have reason to believe that the viscous B_2O_3 formed *in situ* played a key role in healing the fiber's cracks. Besides, melamine and condensed melem displayed a powder state (Fig. S3†), indicating that the solid state remained during heating. This melamine/melem solid could prevent the excessive flow of viscous B_2O_3 and helped avoid the fusion of fibers. In the final stage, the self-healed $M\cdot 2B_{200-400}$ fiber was composed of B_2O_3 glass and melamine/melem.

Moreover, to determine whether the B–O oligomer was uniformly distributed in $M\cdot 2B_{150}$ and B_2O_3 acted as a matrix in $M\cdot 2B_{200-400}$, the fibers underwent corrosion testing by EG (ethylene glycol) and EA (ethanol) considering that B_2O_3 could be rapidly dissolved in EG while remaining stable in EA for a long period. The testing went on merely for 1 minute for avoiding complete dissolution, and the corroded fibers were separately designated as $M\cdot 2B_{T-EG}$ and $M\cdot 2B_{T-EA}$ (T = 150, 200, 400 °C).

As shown in Fig. S5e and f,† all the $M\cdot 2B_{T-EG}$ fibers collapse into pieces due to the severe corrosion in EG. These results disclosed that the B–O oligomer or B_2O_3 was uniform throughout the whole fiber. After 6 hour corrosion, these fibers were completely dissolved, while the $M\cdot 2B_{550}$ fiber remained undissolved due to the predominant BN phase (Fig. S4a†). In contrast, the samples in EA were partially dissolved or undissolved (Fig. S4b†). After being corroded for 1 minute in EA, $M\cdot 2B_{T-EA}$ maintained the fiber's profile (Fig. S5b and S5c†) despite slight etching on the surface of $M\cdot 2B_{150-EA}$, which was composed of parallel short rods (Fig. S5a†) resulting from the decomposition of the intact $M\cdot 2B$ fiber. The partial dissolution of the B–O oligomer at the interface between the rods disclosed this unique morphology.

The cracks in $M\cdot 2B_{150}$ might be the gaps between the mismatched rod bundles. As for $M\cdot 2B_{200-EA}$, the ultrafine fibers generated on the basis of the original $M\cdot 2B_{200}$ fiber (Fig. S5b†) might be attributed to the assembly of $C_3N_6H_6$ and H_3BO_3 (formed *via* the moisture absorption of superficial B_2O_3) in an ethanol solution. $M\cdot 2B_{400-EA}$ maintained the morphology for the initially smooth surface and the inactive melem. In summary, the different corrosion behaviors of the $M\cdot 2B_T$ fibers in EA compared with that in EG confirmed that the B–O oligomer or B_2O_3 was the dominant phase in affecting the fiber's morphology. In other words, B_2O_3 acted as the matrix in the $M\cdot 2B_{200-400}$ fiber in which melamine/melem was enclosed.

On the basis of the above-mentioned discussion, the structural conversion corresponding to "cracking and self-healing" morphology transformation was discussed in detail. The
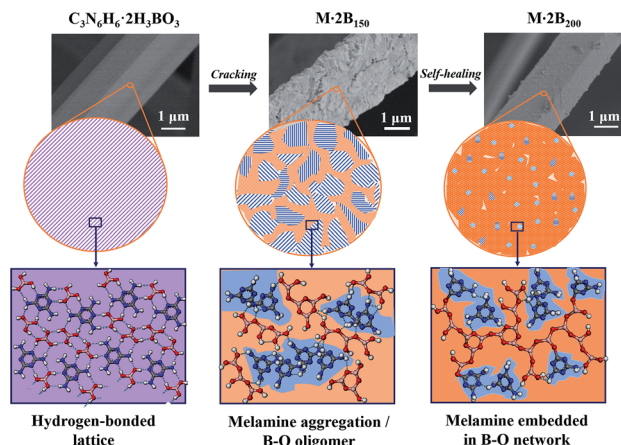

Fig. 4 Schematic illustration of microstructural evolution corresponding to the morphological transformation: cracking and self-healing.

schematic illustration in Fig. 4 shows structure evolution corresponding to the staged morphology. Initially, $M\cdot 2B$ with intact fibrous morphology possessed a hydrogen-bonded lattice, in which $C_3N_6H_6$ and H_3BO_3 were arranged uniformly and orderly. After heating at 150 °C, H_3BO_3 was dehydrated and formed a B–O oligomer, while the $C_3N_6H_6$ molecules aggregated and assembled into tiny crystals. This resulted in the breakage of the ordered hydrogen-bonded structure and the intact fiber decomposed into short-rod bundles. However, the profile of the fiber was maintained integrated owing to the existence of the B–O oligomer at the interface of the rods. As a result, the cracked structure was derived from the mismatched gaps of the bundles. For $M\cdot 2B_{200}$, the extended B_2O_3 network was formed as a result of further dehydration, while the $C_3N_6H_6$ domain shrank and was isolated by the continuous B_2O_3 matrix. Thus, the cracked structure of $M\cdot 2B_{150}$ was healed by the *in situ* viscous matrix. Our results provide a self-healing strategy for inorganic materials, which is different from that for organic polymers involving reversible bonding.[28,29]

To explore the effect of the "self-healing" process on the morphology of the final BN fiber, we treated the $M\cdot 2B$ fibers under different pyrolysis conditions with a stage-variable atmosphere. As shown in Fig. 5, there are three sets of contrasts. In Fig. 5a and b, the BN fiber obtained after treatment under an NH_3 atmosphere is defective, while that obtained under N_2 is smooth in spite of undergoing the same heating process at 1000 °C for 1 hour. The difference in the fiber morphologies could be attributed to "self-healing" between 200 and 400 °C. As is well-known, the complex reaction between B_2O_3 and NH_3 occurs at a temperature close to 200 °C, forming a non-melting $(B_2O_3)_n\cdot NH_3$ compound,[30] which prevents the cracked fiber from self-healing, while the molten B_2O_3 phase formed under a nitrogen atmosphere assists in healing the cracks.

The same comparisons were performed at temperatures lower than 1000 °C. As shown in Fig. 5c and d, the $M\cdot 2B$ green fiber is separately heated under an NH_3 atmosphere and
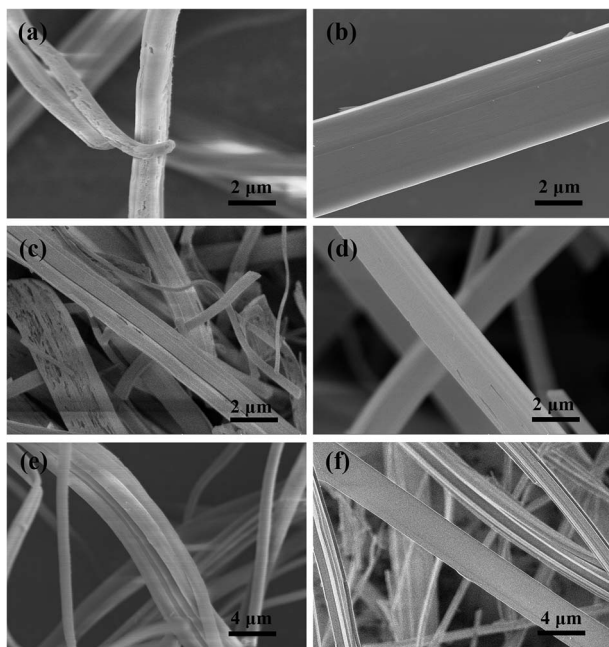
Fig. 5 (a) BN fibers obtained after heating at 1000 °C for 1 hour under NH₃ atmosphere; (b) heating at 1000 °C for 1 hour under N₂ atmosphere; (c) heating at 700 °C for 1 hour under NH₃ and subsequent heating at 1000 °C under N₂; (d) heating at 700 °C for 1 hour in vacuum and subsequent heating at 1000 °C under N₂; (e) heating at 400 °C for 1 hour under NH₃ and heating to 1000 °C under N₂; (f) heating at 400 °C for 1 hour under N₂ and subsequently at 700 °C under NH₃, and finally to 1000 °C under N₂.

vacuum at 700 °C. As shown in Fig. 5e and f, the M·2B green fiber is separately treated at 400 °C under the different combination of NH_3/N_2 atmosphere. Both these comparisons indicated the same results as those obtained from Fig. 5a and b; the fibers pyrolyzed under NH_3 were defective, while the fibers pyrolyzed under N_2 or vacuum were smooth. In summary, the significance of self-healing assisted by the molten B_2O_3 formed at 200 °C is crucial to obtain defect-free BN fibers. The result is of great significance to provide guidance to fabricate dense BN fibers when applying an active atmosphere such as NH_3 for better nitridation and complete removal of carbon.

Conclusions

In summary, the dehydration of H_3BO_3 and evolution of B_2O_3 were figured out to be responsible for the unique "cracking and self-healing" morphological transformation. The resulting fiber was composed of a B_2O_3 matrix, in which melamine/melem was enclosed. This compound structure ensured stable morphology at the subsequent pyrolysis and nitridation stages and laid the foundation for the BN fiber. The self-healing mechanism assisted by the *in situ* molten phase can be adopted to guide the preparation of high-performance M·2B-derived BN fibers and can also be significant for other precursor-derived ceramic materials, especially those with low yields.

Conflicts of interest

There are no conflicts to declare.

Acknowledgements

Notes and references

1 X. Duan, Z. Yang, L. Chen, Z. Tian, D. Cai, Y. Wang, D. Jia and Y. Zhou, *J. Eur. Ceram. Soc.*, 2016, **36**, 3725–3737.

2 J. Eichler and C. Lesniak, *J. Eur. Ceram. Soc.*, 2008, **28**, 1105–1109.

3 T. C. Doan, S. Majety, S. Grenadier, J. Li, J. Y. Lin and H. X. Jiang, *Nucl. Instrum. Methods Phys. Res. Sect. A Accel. Spectrom. Detect. Assoc. Equip.*, 2014, **748**, 84–90.

4 X. Yang, Y. Guo, Y. Han, Y. Li, T. Ma, M. Chen, J. Kong, J. Zhu and J. Gu, *Compos. B Eng.*, 2019, **175**, 1–8.

5 Y. Han, X. Shi, X. Yang, Y. Guo, J. Zhang, J. Kong and J. Gu, *Compos. Sci. Technol.*, 2020, **187**, 107944.

6 T. Ma, Y. Zhao, K. Ruan, X. Liu, J. Zhang, Y. Guo, X. Yang, J. Kong and J. Gu, *ACS Appl. Mater. Interfaces*, 2020, **12**, 1677–1686.

7 Z. Liu, K. Zhao, J. Luo and Y. Tang, *Scr. Mater.*, 2019, **170**, 116–119.

8 V. Salles, S. Bernard, A. Brioude, D. Cornu and P. Miele, *Nanoscale*, 2010, **2**, 215–217.

9 Y. Qiu, J. Yu, J. Rafique, J. Yin, X. Bai and E. Wang, *J. Phys. Chem. C*, 2009, **113**, 11228–11234.

10 Y. P. Lei, Y. De Wang and Y. C. Song, *Ceram. Int.*, 2012, **38**, 271–276.

11 C. Wang, C. Hong, L. Yan, X. Lin, M. Zhang, J. Wang and Q. Qu, *Int. J. Appl. Ceram. Technol.*, 2018, **15**, 660–667.

12 J. Lin, L. Xu, Y. Huang, J. Li, W. Wang, C. Feng, Z. Liu, X. Xu, J. Zou and C. Tang, *RSC Adv.*, 2016, **6**, 1253–1259.

13 C. Wu, B. Wang and Y. Wang, *Ceram. Int.*, 2018, **44**, 5385–5391.

14 G. Li, M. Zhu, W. Gong, R. Du, A. Eychmüller, T. Li, W. Lv and X. Zhang, *Adv. Funct. Mater.*, 2019, **29**, 1–7.

15 P. Miele, S. Bernard, D. Cornu and B. Toury, *Soft Mater.*, 2007, **4**, 249–286.

16 D. Cornu, S. Bernard, S. Duperrier, B. Toury and P. Miele, *J. Eur. Ceram. Soc.*, 2005, **25**, 111–121.

17 Y. P. Lei, Y. De Wang, Y. C. Song and C. Deng, *Ceram. Int.*, 2011, **37**, 3005–3009.

18 C. Deng, Y. Song, Y. Wang, Y. Li and Y. Lei, *Chem. J. Chin. Univ.*, 2010, **31**, 623–628.

19 T. Kawasaki, Y. Kuroda and H. Nishikawa, *J. Ceram. Soc. Jpn.*, 1996, **104**, 935–938.

20 A. Roy, A. Choudhury and C. N. R. Rao, *J. Mol. Struct.*, 2002, **613**, 61–66.

21 J. Lin, X. Yuan, G. Li, Y. Huang, W. Wang, X. He, C. Yu, Y. Fang, Z. Liu and C. Tang, *ACS Appl. Mater. Interfaces*, 2017, **9**, 44732–44739.

22 H. B. Zheng, W. Chen, H. Gao, Y. Y. Wang, H. Y. Guo, S. Q. Guo, Z. L. Tang and J. Y. Zhang, *J. Mater. Chem. C*, 2017, **5**, 10746–10753.

23 X. Gouin, P. Grange, L. Bois, P. L'Haridon and Y. Laurent, *J. Alloys Compd.*, 1995, **224**, 22–28.

24 W. J. Jones and W. J. Orville-Thomas, *Trans. Faraday Soc.*, 1959, **55**, 203–210.

25 C. Y. Panicker, H. T. Varghese, A. John, D. Philip and H. I. S. Nogueira, *Spectrochim. Acta, Part A*, 2002, **58**, 1545–1551.

26 X. Zhang, Z. Lu, H. Liu, J. Lin, X. Xu, F. Meng, J. Zhao and C. Tang, *J. Mater. Chem. C*, 2015, **3**, 3311–3317.

27 S. Wang, C. Bian, B. Jia, Y. Wang and X. Jing, *Polym. Degrad. Stab.*, 2016, **130**, 328–337.

28 X. Yang, Y. Guo, X. Luo, N. Zheng, T. Ma, J. Tan, C. Li, Q. Zhang and J. Gu, *Compos. Sci. Technol.*, 2018, **164**, 59–64.

29 C. Li, J. Tan, J. Gu, L. Qiao, B. Zhang and Q. Zhang, *Compos. Sci. Technol.*, 2016, **123**, 250–258.

30 J. Economy and R. Lin, in *Boron and Refractory Borides*, ed. V. I. Matkovich, Springer Berlin Heidelberg, Berlin, Heidelberg, 1977, pp. 552–564.